Accepted Manuscript

A scalable fully implicit framework for reservoir simulation on parallel computers

Haijian Yang, Shuyu Sun, Yiteng Li, Chao Yang

PII: S0045-7825(17)30686-2
DOI: https://doi.org/10.1016/j.cma.2017.10.016
Reference: CMA 11644

To appear in: *Comput. Methods Appl. Mech. Engrg.*

Received date : 18 June 2017
Revised date : 31 August 2017
Accepted date : 17 October 2017

Please cite this article as: H. Yang, S. Sun, Y. Li, C. Yang, A scalable fully implicit framework for reservoir simulation on parallel computers, *Comput. Methods Appl. Mech. Engrg.* (2017), https://doi.org/10.1016/j.cma.2017.10.016

A scalable fully implicit framework for reservoir simulation on parallel computers

Haijian Yang[a], Shuyu Sun[b,*], Yiteng Li[b], Chao Yang[c,d]

[a] *College of Mathematics and Econometrics, Hunan University, Changsha, Hunan 410082, PR China*
[b] *Physical Science and Engineering Division, King Abdullah University of Science and Technology, Thuwal, 23955-6900, Saudi Arabia*
[c] *Institute of Software, Chinese Academy of Sciences, Beijing 100190, PR China*
[d] *State Key Laboratory of Computer Science, Chinese Academy of Sciences, Beijing 100190, PR China*

Abstract

The modeling of multiphase fluid flow in porous medium is of interest in the field of reservoir simulation. The promising numerical methods in the literature are mostly based on the explicit or semi-implicit approach, which both have certain stability restrictions on the time step size. In this work, we introduce and study a scalable fully implicit solver for the simulation of two-phase flow in a porous medium with capillarity, gravity and compressibility, which is free from the limitations of the conventional methods. In the fully implicit framework, a mixed finite element method is applied to discretize the model equations for the spatial terms, and the implicit Backward Euler scheme with adaptive time stepping is used for the temporal integration. The resultant nonlinear system arising at each time step is solved in a monolithic way by using a Newton–Krylov type method. The corresponding linear system from the Newton iteration is large sparse, nonsymmetric and ill-conditioned, consequently posing a significant challenge to the fully implicit solver. To address this issue, the family of additive Schwarz preconditioners is taken into account to accelerate the convergence of the linear system, and thereby improves the robustness of the outer Newton method. Several test cases in one, two and three dimensions are used to validate the correctness of the scheme and examine the performance of the newly developed algorithm on parallel computers.

Keywords: Reservoir simulation, Fully implicit method, Schwarz preconditioner, Parallel computing

1. Introduction

Reservoir simulation models are used extensively by oil and gas industries to efficiently manage existing petroleum fields and to develop new oil and gas reservoirs [1, 9]. Although

*Corresponding author.
Email addresses: haijianyang@gmail.com (Haijian Yang), shuyu.sun@kaust.edu.sa (Shuyu Sun), yiteng.li@kaust.edu.sa (Yiteng Li), yangchao@iscas.ac.cn (Chao Yang)

reactive transport modeling in porous media is more realistic which have been discussed in[36, 37, 38], most reservoir simulations more focus on advection [32, 19], as well as diffusion [15]. In order to represent complex geological heterogeneity and to capture highly spatially varying solutions for Darcy velocity, saturation, and concentration, it is common to use millions (or even billions) of grid blocks or cells in large-scale geological models for field-scale flow and transport simulation. Additional computational challenges come from the complexity of the geological media, the flowing fluid, and their interaction, which demands robust and efficient computation of subsurface flow and transport. To address these challenges, parallel reservoir simulators equipped with robust, scalable and efficient algorithms are essential to improve simulation runs and simulators capability.

The modeling equations of multiphase flow in geological formation typically include conservation laws for each phase (for fully immiscible multiphase flow) or conservation laws for each component (for partially miscible multiphase flow). In addition, extended Darcy's law is usually assumed for multi-phase flow in the media. This phenomenological law together with conservation laws and fluid properties are often used to model the fluid flow behaviors in the subsurface system. Numerical solution procedure involves approximation using spatial and temporal discretization. Finite difference, finite volume, or finite element methods can be used for spatial discretization. The local conservation property of the discretization scheme is often important. Popular conservative methods include the block-centered finite difference method and the Raviart-Thomas mixed finite element method.

Various decoupled splitting schemes and time integration schemes have been used to discretize the equation system in time and to tackle the coupled equations. The simplest and most straightforward approach is to treat all terms explicitly, e.g. as in the forward Euler method. These fully explicit methods are easy to implement and computationally cheap for a single time step; however, governing equations for multiphase flow often come with strong nonlinearity and stiffness, leading to the severe Courant-Friedrichs-Lewy (CFL) condition [11]. As a result, the explicit methods become prohibitively expensive due to the tiny time steps imposed by the CFL condition. Semi-implicit methods have been widely used in practice because of its improved stability over the fully explicit methods. One popular semi-implicit scheme people use in practice is the IMPES (implicit in pressure and explicit in saturation) scheme [8, 11, 12, 20, 48]. The motivation of IMPES comes from the observation that the pressure and Darcy's velcoity changes less rapidly with time as compared with the phase saturation or species concentration. In the iterative IMPES scheme [27, 29, 30], a number of iterations are performed in a single pressure-saturation time step interval to increase its accuracy and/or stability. It can be considered as an improved version of IMPES or as an iterative solution procedure of a fully implicit scheme. In spite of the popularity of semi-implicit methods, it is believed in computational community that the most promising scheme for subsurface multi-phase flow is the fully implicit method [1, 10, 14, 31, 39, 41, 49], mainly because of its unconditionally stability. In the fully implicit approach, all the coupled nonlinear equations are solved simultaneously and implicitly, thereby the whole system approach has the potential to allow more physics to be added easily to the system without changing much of the algorithmic and software framework.

Even though being stable for arbitrary large time steps, the computational efficiency of

a fully implicit method still relies on sophisticated nonlinear and linear solvers, especially when the size of problems becomes large. It remains challenging and important to obtain efficient nonlinear and linear solvers of the algebraic systems arising from the fully implicit treatment of reservoir simulation. In this study, we propose a highly parallel solver based on the framework of Newton–Krylov–Schwarz (NKS) algorithms [4, 6, 22, 25, 43] to guarantee the nonlinear consistency. In the proposed NKS method, the resultant nonlinear system is solved by a generalized Newton method, i.e., active-set reduced-space method [3, 23, 47], and then the linear Jacobian systems are solved with a preconditioned Krylov subspace method. The success of the overall approach depends heavily on the preconditioner, owing to the fact that it can substantially reduce the condition number of the linear system. Hence, we use the overlapping additive Schwarz type domain decomposition methods [17, 35, 40] to build the preconditioner. A great advantage of domain decomposition methods is that communication only occurs between neighboring subdomains during the restriction and extension processes, and meanwhile does not require any splitting of the nonlinear system. Therefore the additive Schwarz preconditioner is naturally suitable to massively parallel computing and provides the scalability. In particular, with the appearance of the restricted version of Schwarz methods proposed by Cai and Sarkis in [7], it can lead to substantial reduction of the total computing time, which greatly expands the scope of application of the domain decomposition algorithm. An important implementation detail in designing the additive Schwarz preconditioner is to balance the quality of the iterations and the computing time spent on the simulation. Hence, several performance-related parameters in the preconditioner, including the type of the Schwarz preconditioner and the size of the overlap, are carefully discussed and tested to achieve the optimal performance. By using these strategies, our experiments show that the proposed fully implicit solver based on the Newton–Krylov–Schwarz algorithm is efficient, robust and scalable on a supercomputer.

The remainder of the paper is organized as follows. In Section 2, we introduce the mathematical model for the two-phase slightly compressible flow, following which a fully implicit scheme is provided for the temporal and spatial discretization. In Section 3, we briefly review the Newton–Krylov type method with additive Schwarz preconditioners for solving the resultant nonlinear system. Several sets of numerical experiments with parallel performance results are reported in Section 4 and the paper is concluded in Section 5.

2. Mathematical model and discretization

Consider a time interval $[0, T]$ and a spatial domain $\Omega \subset \mathbb{R}^d$, $d = 1, 2$ or 3, with boundary $\partial\Omega$. The model of the two-phase slightly compressible flow through a porous medium is described by the continuity equation and the Darcy law of the wetting and the non-wetting fluid phases. Let the subscripts o and w denote the non-wetting and wetting phases, respectively. The continuity equation of the phase $\alpha = o, w$ is given by

$$\frac{\partial}{\partial t}(\phi \rho_\alpha S_\alpha) + \nabla \cdot (\rho_\alpha u_\alpha) = q_\alpha, \tag{1}$$

where ϕ is the porosity of the medium, S_α is the saturation, ρ_α is the density, q_α is the external mass flow rate, and u_α denotes the volumetric velocity of phase α. The velocity u_α

is described by the Darcy law as follows:

$$u_\alpha = -\frac{k_{r\alpha}}{\mu_\alpha}\mathbf{K}\left(\nabla p_\alpha + \rho_\alpha g \nabla z\right) \tag{2}$$

where $\mathbf{K}$ is the absolute permeability tensor, $p_\alpha, k_{r\alpha}$ and μ_α are pressure, relative permeability, and viscosity, respectively. Moreover, g is the gravity acceleration constant and z is the depth. The void of porous medium is jointly filled by the two fluids, and the relation of their saturations satisfies the following constraints

$$S_w + S_o = 1. \tag{3}$$

The relation between the wetting and non-wetting phase pressures is given by the capillary pressure [9, 24],

$$p_c(S_w) = p_o - p_w, \tag{4}$$

which is a known function of the wetting phase saturation that relates the two phase pressures. In addition to that, the density ρ_α is given by

$$\rho_\alpha = \hat{\rho}_\alpha e^{c_\alpha (p_\alpha - \hat{p})}, \tag{5}$$

which describes the slightly compressible density of each phase with small compressibility constants c_α, the reference density $\hat{\rho}_\alpha$ and the reference pressure $\hat{p}$. In this paper, the primary variables to be solved in (1) are the wetting-phase pressure p_w and saturation S_w. The boundary conditions are assumed to be impervious, i.e., for the both phases o and w, the velocity $u_\alpha = 0$. The injection and production wells are respectively modeled as the inflow and the outflow boundaries [9].

In this study, we use a mixed finite element method for the spatial discretization and a backward differentiation formula with adaptive time stepping for the temporal integration, as introduced in the Appendix. After applying the fully implicit scheme, the equations (1) is discretized into a nonlinear system

$$F(X) = \begin{pmatrix} F^{(p_w)}(X) \\ F^{(S_w)}(X) \end{pmatrix} = 0, \tag{6}$$

where $X = (p_w, S_w)^T$ for each time step.

We remark that a popular approach for describing the mathematical model is based on the pressure equation and one of the continuity equations, see references [24, 26, 31, 44] for more details. However, in this treatment, the mass conservation of the other phase might not be guaranteed, since the saturation is calculated by the volume constraint instead of solving its continuity equation. Hence, in this study, we use an alternative and different formulation for describing the continuity of the two-phase flow in a porous medium. Two continuity equations, which naturally satisfy the mass conservation of the two phases, are solved simultaneously. A particular emphasis of this formulation is that the upwind scheme can be applied to both continuity equations. Consequently, the latter approach can capture the direction of information propagation in the flow field and thereby overcome nonphysical oscillations in the simulation.

3. Parallel fully implicit solver

The implicit discretization of (1) gives rise to nonlinear systems of equations, which are normally solved with the class of Newton methods [18, 34, 41]. However, when solving such nonlinear systems using the classical Newton methods, we often face the numerical challenges arising from physically feasible saturation fractions between S_b and S_u, i.e., $S_b \leq S_w \leq S_u$. Hence, we introduce a constrained optimization based formulation with a box inequality constraint, which naturally satisfies the boundedness requirement. Then we employ a generalized Newton–Krylov method with additive Schwarz preconditioners to solve the corresponding nonlinear algebraic systems efficiently on parallel supercomputers.

3.1. Constrained optimization based formulation

For the saturation component, a constrained optimization problem is introduced when the constraint condition $S_b \leq S_w \leq S_u$ is considered

$$\begin{cases} \min \mathcal{J}(S_w) \\ \text{s.t. } S_b \leq S_w \leq S_u, \end{cases} \tag{7}$$

where $\mathcal{J}(S_w)$ is continuously differentiable defined by

$$\nabla \mathcal{J}(S_w) = \frac{\partial \mathcal{J}(S_w)}{\partial S_w} = F^{(S_w)}(X).$$

With the help of the Lagrange multipliers λ_{S_b} and λ_{S_u} for the restrictions, a Lagrangian function is defined as

$$\mathcal{L}(S_w, \lambda_{S_b}, \lambda_{S_u}) \equiv \mathcal{J}(S_w) + (S_b - S_w, \lambda_{S_b}) + (S_w - S_u, \lambda_{S_u}). \tag{8}$$

Then the first-order optimally conditions are obtained by differentiating (8)

$$\begin{cases} F^{(S_w)}(X) - \lambda_{S_b} + \lambda_{S_u} = 0, \\ S_b - S_w \leq 0, \lambda_{S_b} \geq 0, (S_b - S_w, \lambda_{S_b}) = 0, \\ S_w - S_u \leq 0, \lambda_{S_u} \geq 0, (S_w - S_u, \lambda_{S_u}) = 0. \end{cases} \tag{9}$$

Finally, we can obtain the following variational inequality by eliminating Lagrange multipliers λ_{S_b} and λ_{S_u} in (9)

$$\begin{cases} S_w = S_b & \& \quad F^{(S_w)}(X) \geq 0, \\ S_w = S_u & \& \quad F^{(S_w)}(X) \leq 0, \\ S_w \in (S_b, S_u) & \& \quad F^{(S_w)}(X) = 0. \end{cases} \tag{10}$$

Similarly, we also build a variational inequality formulation for the pressure component

$$\begin{cases} p_w = -\infty & \& \quad F^{(p_w)}(X) \geq 0, \\ p_w = +\infty & \& \quad F^{(p_w)}(X) \leq 0, \\ p_w \in (-\infty, +\infty) & \& \quad F^{(p_w)}(X) = 0. \end{cases} \tag{11}$$

We would like to point out that, although there are not any restriction for the pressure p_w, i.e., $-\infty < p_w < +\infty$, the purpose of (11) is to obtain a constrained optimization based formulation for the coupled system (6), which is defined as follows. Let $\mathcal{S} = \{1, 2, \cdots, N\}$ be an index set with each index corresponding to an unknown component X_i and a nonlinear residual component F_i. Suppose the lower- and upper-bound vectors for the solution X are respectively defined by

$$\begin{cases} \phi = (-\infty, S_b, \cdots, -\infty, S_b, \cdots, -\infty, S_b) = (\phi_1, \phi_2, \cdots, \phi_N) \in \mathbb{R}^N, \\ \psi = (+\infty, S_u, \cdots, +\infty, S_u, \cdots, +\infty, S_u) = (\psi_1, \psi_2, \cdots, \psi_N) \in \mathbb{R}^N. \end{cases} \tag{12}$$

Then, by coupling the systems (10) and (11), the variational inequality for (6) is defined as follows: find a vector $X \in \mathbb{R}^N$ such that only one of the following three equations holding at a time

$$\begin{cases} X_i = \phi_i & \& \quad F_i(X) \geq 0, \\ X_i = \psi_i & \& \quad F_i(X) \leq 0, \\ X_i \in (\phi_i, \psi_i) & \& \quad F_i(X) = 0. \end{cases} \tag{13}$$

3.2. Newton–Krylov type algorithm

We employ a family of Newton–Krylov methods with additive Schwarz preconditioners to solve (13) efficiently on supercomputers. The proposed algorithm consists of three important components: (1) an active-set reduced-space method for the nonlinear system; (2) a Krylov iterative method for the linear Jacobian system at each Newton iteration; and (3) a Schwarz preconditioner for the linear solver.

First, let us discuss some details about the active-set reduced-space method for a given nonlinear system. Let the operator π be a projection to cut off the undershoot or overshoot of the solution from the interval $[\phi, \psi]$. Suppose X^k is the current approximate solution, then a new approximate solution X^{k+1} can be computed through the following steps:

1. Determine the active sets $\mathcal{I}_\phi(X^k)$ and $\mathcal{I}_\psi(X^k)$ by

$$\begin{cases} X_i^k = \phi_i & \& \quad F_i(X^k) \geq 0, \quad \text{on } \mathcal{I}_\phi(X^k), \\ X_i^k = \psi_i & \& \quad F_i(X^k) \leq 0, \quad \text{on } \mathcal{I}_\psi(X^k), \end{cases} \tag{14}$$

   and then define the inactive set by $\mathcal{I}_\phi(X^k) = \mathcal{S} \setminus \big(\mathcal{I}_\psi(X^k) \cup \mathcal{I}(X^k)\big)$.

2. Set $d_{\mathcal{I}_\phi} = 0$ and $d_{\mathcal{I}_\psi} = 0$, and compute a direction $d_{\mathcal{I}}$ by approximately solving the linear system by a relative tolerance $\eta_r \in [0, 1)$, an absolute tolerance $\eta_a \in [0, 1)$ and the condition

$$\Big\| \big[\nabla F(X^k)\big]_{\mathcal{I},\mathcal{I}} d_{\mathcal{I}} + F_{\mathcal{I}}(X^k) \Big\| \leq \max\left\{ \eta_r \|F_{\mathcal{I}}(X^k)\|, \eta_a \right\}, \tag{15}$$

   where $\big[\nabla F(X^k)\big]_{\mathcal{I},\mathcal{I}}$ is a submatrix of $\nabla F(X^k)$ and $F_{\mathcal{I}}(X^k)$ is a subvector of $F(X^k)$, both based on the same index set $\mathcal{I}$.

3. Set $X^{k+1} = \pi\left[X^k + \lambda^k d^k\right]$, where $\lambda^k \in (0, 1]$ is determined to satisfy

$$\left\| F_\Theta\left(\pi\left[X^k + \lambda^k d^k\right]\right) \right\| \leq (1 - \alpha\lambda^k)\left\| F_\Theta(X^k)\right\|, \tag{16}$$

with $F_\Theta(X)$ being defined as

$$[F_\Theta(X)]_i = \begin{cases} F_i(X), & \text{if } \phi_i < X_i < \psi_i, \\ \min\{F_i(X), 0\}, & \text{others.} \end{cases}$$

4. We continue the nonlinear iteration until the following convergence criterion is satisfied

$$||F_\Theta(X^k)|| \leq \max\{\varepsilon_r ||F_\Theta(X^0)||, \varepsilon_a\},$$

where ε_r (ε_a) is the relative (absolute) solver tolerance for the nonlinear iteration.

Remark 1 *When combined with Krylov–Schwarz method, the active-set reduced-space method degrades into the classical Newton–Krylov–Schwarz (NKS) [4, 6, 22, 25, 43] for the case that the active sets in* (14) *are all through empty, i.e.,* $\mathcal{I}_\phi(X) = \mathcal{I}_\psi(X) = \emptyset$.

Remark 2 *The parameter* λ^k *in* (16) *is used to assure that the reduction of the residual function is sufficient. For the simulation of two-phase flow in porous media using the active-set reduced-space method, if* λ^k *doesn't satisfy the descend condition in* (16)*, then we update the initial guess* X^k *by solving the following nonlinear system with the NKS method:*

$$\tilde{F}(X) = \begin{pmatrix} X_{(p_w)} - X^k_{(p_w)} \\ F^{(S_w)}(X) \end{pmatrix} = 0, \tag{17}$$

where $X_{(p_w)}$ *is the subvector with respect to the variable* p_w*. The purpose of this step is to keep the part of* X^k *with respect to* p_w*, while the other part with respect to* S_w *is replaced by solving* $F^{(S_w)}(X) = 0$.

3.3. Additive Schwarz preconditioner

In the above method, the Newton correction vector d^k is used to determine the step length that one should go in the selected nonlinear correction direction, which is obtained by solving a linear Jacobian system. Compared to the classical exact method, the inexact method has some potential advantages for large-scale computing, i.e., the number of unknowns is large (e.g., of the order of millions or larger), due to the reason that the inexact treatment of the linear system leads to a substantial reduction of the computational cost [21]. More importantly, the linear system is solved approximately instead of exactly can avoid the over solving problems of Newton type methods and hence improve the efficiency. In the proposed fully implicit solver, the linear system is solved by using a Krylov subspace method [33]. In practice, the overlapping additive Schwarz preconditioned Generalized Minimal RESidual (GMRES) method that restarts every 90 iterations is employed in our solver.

In large-scale parallel computing, the additive Schwarz preconditioner is the key to the success of the linear solver, since it can help in improving the convergence and meanwhile is

beneficial to the scalability of the linear solver. To define this domain decomposition based preconditioner, we assume that $\Omega \subset \mathbb{R}^d$, $d = 1, 2$ or 3, is covered by the non-overlapping and overlapping partitions as shown in Figure 1. Let J be the Jacobian matrix of the nonlinear problem and let R_i^δ and R_i^0 be the restriction operator from Ω to its overlapping and non-overlapping subdomains, respectively. Here, the parameter δ denotes the size of the overlap. Then the classical additive Schwarz (AS, [17]) preconditioner is defined as

$$M_{\delta,\delta}^{-1} = \sum_{i=1}^{N_p} (R_i^\delta)^T J_i^{-1} R_i^\delta. \tag{18}$$

with $J_i = R_i^\delta \; J \; (R_i^\delta)^T$ and N_p is the number of subdomains, which is the same as the number of processors. In addition to that, there are two modified approaches of the additive Schwarz preconditioner that may have some potential advantages for parallel computing. The first version is the left restricted additive Schwarz (left-RAS, [7]) method defined by

$$M_{0,\delta}^{-1} = \sum_{i=1}^{N_p} (R_i^0)^T J_i^{-1} R_i^\delta. \tag{19}$$

and the other modification to the original method is the right restricted additive Schwarz (right-RAS, [5]) preconditioner as follow:

$$M_{\delta,0}^{-1} = \sum_{i=1}^{N_p} (R_i^\delta)^T J_i^{-1} R_i^0. \tag{20}$$

Note that, in practice, we use a sparse LU factorization based direct method to solve the subdomain linear system corresponding to the matrix J_i^{-1} in (18), (19) or (20).

A great advantage of the additive Schwarz preconditioners is that communication only occurs between neighboring subdomains during the restriction and extension processes, which is naturally suitable to parallel computing. We would like to point out that, for the preconditioners (19) and (20), the operator R_i^δ is replaced by R_i^0, as a result the corresponding part of the computation will not require any communication because the image of R_i^0 does not overlap. Therefore, compared to the classical additive Schwraz preconditioner, the communication in the two restricted versions is reduced, and this may result in less overall convergence time and further improve the performance of the preconditioner [7]. Some numerical results will be shown later to compare the performance of these preconditioners.

Remark 3 *If an additive Schwarz preconditioner is used to solve an elliptical problem, then the condition number κ of the preconditioned linear system satisfies the following inequality:*

$$\kappa \leq C(1 + H/\delta)/H^2,$$

where H is the subdomain size and C is independent of δ, H, and the mesh size h; see [7, 35, 40] and the references within. Theoretically, this condition number estimate can not be applied immediately to the family of hyperbolic equations such as the two-phase flow problem. As a result, there are very little theoretical literatures on the convergence of domain

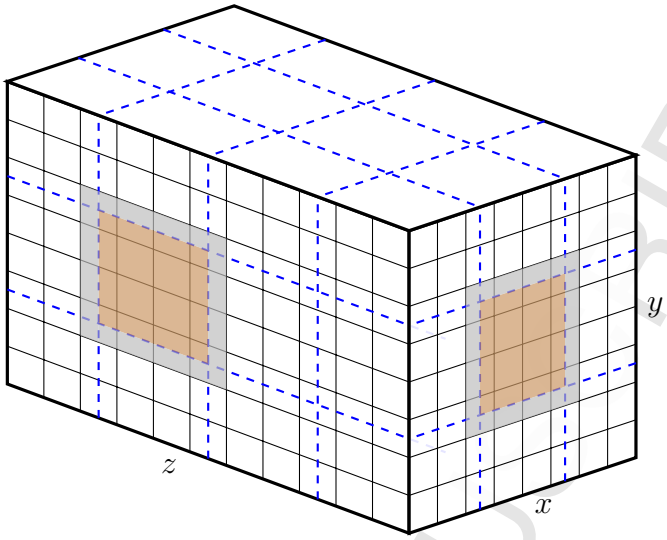

Figure 1: A demonstrated partition of a 3D domain into $3 \times 3 \times 4$ subdomains with $\delta = 1$ by using the blue dashed line. In the figure, the brown part denotes the non-overlapping subdomain, and the grey part denotes the overlap.

decomposition methods for the hyperbolic system. Some numerical results for the Euler equations [16, 43] and the transport problem [45, 46] suggest that the condition number growth of the linear system preconditioned by the additive Schwarz method for the hyperbolic system is less severe than for the elliptic case. Hence, in this study we test some numerical experiments to provide more understanding of the Schwarz method for the two-phase flow problem.

4. Numerical experiments

We implement the algorithms studied in this paper using the open-source Portable, Extensible Toolkit for Scientific computation (PETSc) library ([2]) that is built on the top of Message Passing Interface (MPI). The numerical tests are carried out on the Tianhe-2 supercomputer. The computing nodes of Tianhe-2 are interconnected via a proprietary high performance network, and there are two 12-core Intel Ivy Bridge Xeon CPUs and 24GB local memory in each node. The Intel Xeon Phi coprocessors are not utilized in our tests. In the numerical experiments, we use all 24 CPU cores in each node and assign one subdomain to each core. In the fully implicit solver, we set the tolerances as follows. For the nonlinear iteration, an absolute (relative) tolerance of 10^{-8} (10^{-6}) is utilized. For the linear iteration, the linear systems are solved by the Schwarz preconditioned GMRES method with absolute and relative tolerances of 10^{-6} and 10^{-4}, respectively. In our fully implicit solver, the adaptivity parameters α and γ in (A.1) are set to 2.5 and 0.75, respectively.

In our tests, we use the following parameters if it is not specifically stated. The absolute permeability tensor in (2) is defined as $\mathbf{K} = kI$, where I is the identity matrix and k is a positive real number. The residual saturations for the wetting and non-wetting phases are

S_{rw} and S_{ro}, respectively. The normalized saturation $S_e \in (0,1)$ is defined as

$$S_e = \frac{S_w - S_{rw}}{1 - S_{rw} - S_{ro}},$$

The relative permeabilities in (2) are given by

$$\begin{cases} k_{rw} = S_e^{\beta}, \\ k_{rn} = (1 - S_e)^{\beta}, \end{cases} \tag{21}$$

where β is a positive integer number. The capillary pressure function in (4) is given by

$$p_c = \frac{B_c}{\sqrt{k}} \log(S_e), \tag{22}$$

where B_c is a positive parameter. Both wells are vertical and completed through the entire reservoir depth. In the constrained optimization based formulation, the upper and lower bounds in (12) are fixed to $S_b = 0$ and $S_u = 1$ for all the test cases, except for Case-4 where we set $S_b = 0.2$ and $S_u = 1$.

4.1. Numerical validation

In this subsection, we validate the discretization scheme and the fully implicit solver by running previously published test case. We first verify our numerical model with known analytical solutions in one-dimension space. In the first test case (Case-1), the Buckley-Leverett flow in a 1D domain with constant porosity (0.2) and absolute permeability (100 md) is considered [42]. Initially, the entire domain is fully saturated with oil. Water is uniformly injected from the left hand side of the domain and oil is produced from the opposite right hand side. Other relevant parameters are shown in Table 1.

Table 1: Relevant data for Case-1.

Parameters	Case-1
Domain dimensions	$L = 1\,\mathrm{m}$
Rock properties	$\phi = 0.2, k = 100\mathrm{md}$
Fluid properties	$\mu_w = 1\,\mathrm{cp}, \mu_n = 5\,\mathrm{cp}$
Residual saturations	$S_{rw} = 0, S_{rn} = 0$
Injection rate	$10^{-5}\,\mathrm{m}^3/\mathrm{s}$

The purpose of this test case is to show the correctness of the discretization scheme with different inclination angles θ. Here, the inclination angle is defined by the counter-clockwise angle between the flow direction and the horizontal direction. In this case, the gravity acts as resistance as fluids flow. A fixed time step $\Delta t = 0.1\,\mathrm{s}$ is used and the simulation is stopped at $t = 81\,\mathrm{second}$. The mesh sizes are ranged from 100, 200 to 500. Figure 2 shows the comparison of the wetting phase saturation profiles with different inclination angles. The shock front saturations for Figure 2 is 0.49. However, the shock front distance for the case of

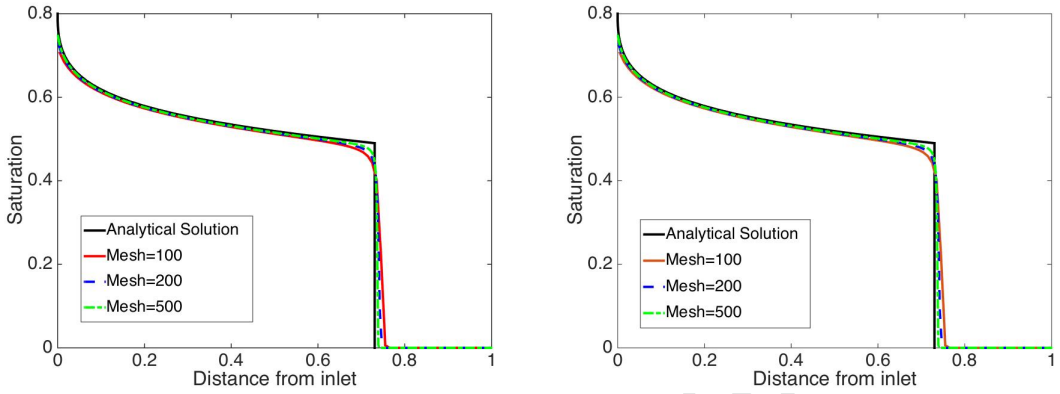

(a) $\theta = 0°$ (b) $\theta = 60°$

Figure 2: The profile curves of the wetting phase saturation with inclination angle $\theta = 0°$ and $\theta = 60°$ for Case-1.

$\theta = 60°$ is slightly less than that for the case of $\theta = 0°$ (0.7307 m) because the wetting phase has to overcome the gravity effect as it flows. It is clearly seen the computed saturation profiles converge to the analytical solution as the mesh is refined.

To further validate our numerical model, a more complex example (Case-2), proposed by [42], is used which extends the Buckley-Leverett flow in a heterogeneous porous medium. The 1D domain is composed of two different permeabilities (100 md and 10 md), i.e.,

$$k = \begin{cases} 100\,\text{md}, & 0 \le L \le 0.5, \\ 10\,\text{md}, & 0.5 < L \le 1. \end{cases}$$

The relative permeabilities of wetting phase and non-wetting phase in each domain have the following forms

$$\begin{aligned} k_{rw,1} &= 1.831 S_w^4, \\ k_{rn,1} &= 0.75\left(1 - 1.25 S_w\right)^2 \left(1 - 1.652 S_w^2\right), \\ k_{rw,2} &= 0.4687 S_w^2, \\ k_{rn,2} &= 0.25\left(1 - 1.25 S_w\right)^2, \end{aligned}$$

where S_w is water saturation and subscript 1 and 2 represent the subdomain with 100 md and the subdomain with 10 md, respectively. In this test, we ignore capillary pressure and use the same well pattern as Case-1. Parameters for the extended Buckley-Leverett flow are provided in Table 2.

The purpose of this test is to show the capability of the proposed model to simulate an immiscible two-phase flow in a composite system. In the left of Figure 3, we reproduce the profile curve of the wetting phase saturation in [42] to a great extent. The water saturation at the interface of the domain $[0, 0.5]$ is 0.5165 and the corresponding water saturation

Table 2: Relevant data for Case-2.

Parameters	Case-2
Domain dimensions	$L_1 = 0.5\,\text{m}, L_2 = 0.5\,\text{m}$
Rock properties	$\phi = 0.2, k = 100,\ 10\,\text{md}$
Fluid properties	$\mu_w = 1\,\text{cp}, \mu_n = 5\,\text{cp}$
Residual saturations	$S_{rw} = S_{rn} = 0$
Injection rate	$10^{-5}\,\text{m}^3/\text{s}$

at the interface of the domain $[0.5, 1]$ is 0.4717. It is clear the proposed model captures the saturation discontinuity at the interface of porous media ($L = 0.5$) very well. With the grid refinement, the discontinuity and the shock front can be improved. We further compare our numerical solutions with the analytical solution by changing permeability ratio and inclination angle. In the right of Figure 3, we illustrate the profile of wetting phase saturation in a composite porous medium where the absolute permeabilitis are 1000 md and 10 md and the inclination angle is -60 degree. We do not show the figure corresponding to the same absolute permeabilities (1000 md and 10 md) but with zero inclination angle, because saturation profiles of the horizontal flow are completely independent of absolute permeabilities. Thus, the left part of Figure 3 also applies to the case of $k_1/k_2 = 100$ and $\theta = 0°$. Under the gravity effect, the water saturation at the interface of $[0, 0.5]$ increases to 0.5174 but the water saturation at the interface of $[0.5, 1]$ slightly decreases to 0.4709. From these figures, we verify the performance of the proposed model and find it is satisfying.

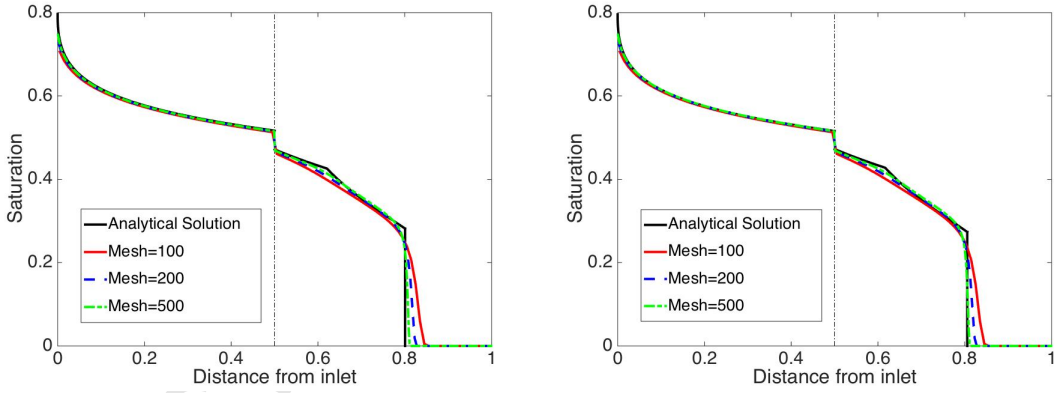

(a) $k_1/k_2 = 10$, $\theta = 0°$ (b) $k_1/k_2 = 100$, $\theta = 60°$

Figure 3: The profile curves of the wetting phase saturation with different permeability ratios and inclination angles for Case-2.

The third test case (Case-3), proposed by [24, 26], describes a 2D horizontal domain that

is composed of layers of alternate permeabilities (1 md and 100 md), i.e.,

$$k = \begin{cases} 1 \text{ md} & 50 \leq y \leq 100, \\ 100 \text{ md} & \text{otherwise.} \end{cases}$$

In the whole domain, the void of medium is initially fully saturated with oil (non-wetting phase), and then water (wetting phase) is uniformly injected from the injection well located at the left hand side of the domain. The oil is across the production well in the opposite right hand side. Other relevant parameters are shown in Table 3. We perform the mesh convergence test to assure our numerical solutions with good quality by using the mesh sizes ranging from 100×50 to 400×200 at 0.4 pore volume injection (PVI). In this test, we use a fixed time step $\triangle t = 10^{-3}$ and finish the simulation at $t = 2$ year. Figure 4 illustrates a set of the plots for profile curves of the wetting-phase saturation along the vertical sections $y = 75$ and $y = 100$ with different mesh sizes. From these figures, we find that the computed saturation profiles are stable and converge as the mesh is refined.

Table 3: Relevant data for Case-3.

Parameters	Case-3
Domain dimensions	300 m $\times$ 150 m
Rock properties	$\phi = 0.2$, $k = 1,100$ md
Fluid properties	$\mu_w = 1$ cP, $\mu_o = 0.3$ cP,
Relative permeabilities	$\beta = 3$ in (21)
Capillary pressure	$B_c = 60$ Bar in (22)
Residual saturations	$S_{rw} = 0, S_{rn} = 0$
Injection rate	0.2 PV/year
Compressibilities	$c_w = 3 \times 10^{-4}$, $c_o = 2 \times 10^{-4}$
Reference densities	$\rho_w^{\text{ref}} = 1000$ kg/m^3, $\rho_0^{\text{ref}} = 660$ kg/m^3

4.2. Effect of wells and capillarity on flow in heterogeneous media

The Tenth SPE Comparative Project [13] is a challenging test case due to the highly heterogeneous permeability and porosity. The 26th layer is used here, whose permeability is ranged from 6.65×10^{-4} md to 2×10^4 md and the value of the porosity belongs to $[0, 0.5]$, as shown in Figure 5. It dimensions are 1200 ft $\times$ 2200 ft. Numerical simulation of fluids flow if any type in petroleum reservoirs must account for the presence of the wells. The purpose of this test case (Case-4) is to show the robustness of the proposed method with different injection and production wells. We consider two different configurations for the wells. In the first configuration (Model-1), the injection well is located at the left hand side of the domain and the oil is across the production well in the opposite right hand side; and in the second configuration (Model-2), the injection and production wells are located at the coordinates $(0, 0)$ and $(1200 \text{ ft}, 2200 \text{ ft})$, respectively. The rock and fluid properties are provided in Table 4.

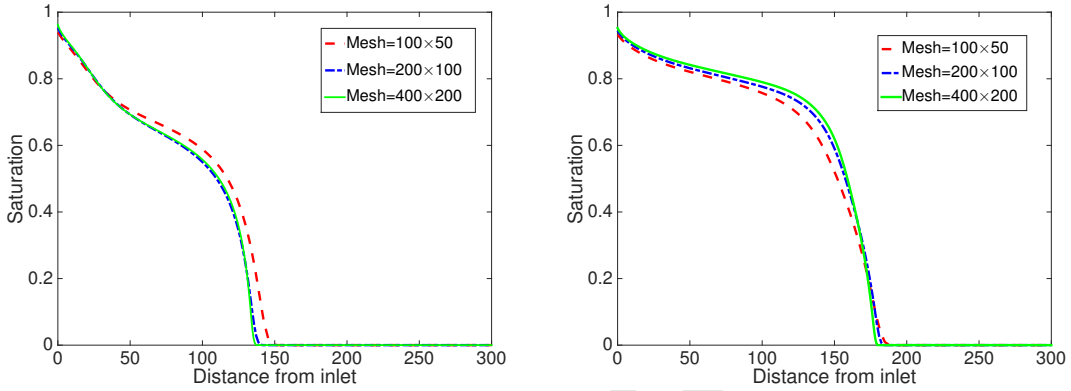

(a) $y = 75$ (b) $y = 100$

Figure 4: The profile curves of the wetting-phase saturation on the along $y = 75$ and $y = 100$ for Case-3.

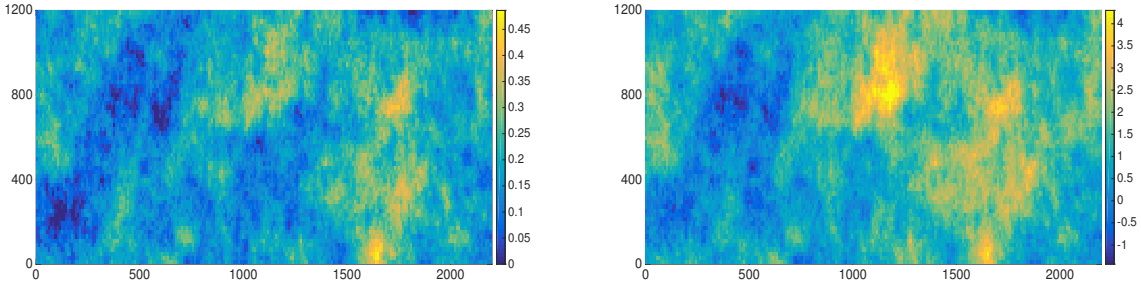

(a) Porosity (b) Permeability

Figure 5: Porosity and permeability for Case-4. We use the logarithmic scale for the permeability, i.e., $\log(k)$ where k has a unit of md.

Table 4: Relevant data for Case-4.

Parameters	Case-4
Domain dimensions	1200 ft $\times$ 2200 ft
Rock properties	$\phi \in [0, 0.5]$, $k \in [6.65 \times 10^{-4}, 2 \times 10^{4}]$ md
Fluid properties	$\mu_w = 0.3$ cP, $\mu_o = 3$ cP,
Relative permeabilities	$\beta = 2$ in (21)
Capillary pressure	$B_c = 0, 20$ Bar in (22)
Residual saturations	$S_{rw} = 0.2, S_{rn} = 0.2$
Injection rate	0.01 PV/year
Compressibilities	$c_w = 3 \times 10^{-4}$, $c_o = 2 \times 10^{-4}$
Reference densities	$\rho_w^{\text{ref}} = 1000$ kg/m^3, $\rho_0^{\text{ref}} = 660$ kg/m^3

In the two-phase immiscible flow, the capillary pressure of heterogenous permeable media is a significant factor on the effect of the flow path. The discontinuity of the capillary, which arises from the discontinuity in the saturation and the contrast in the capillary pressure function, leads to complications in numerical modelling. In this test case, we show the importance of capillary pressure contrast in heterogeneous media. As shown in the figure, the injected water flow is faster in the more permeable layers if the capillary pressure is neglected, i.e., the parameter $B_c = 0$ in (22). In this case, the capillary pressure defined in (4) is a continuous function because its threshold value is zero. On the other hand, when we take the capillary pressure into account, the flow in the more permeable layers slows down because of the cross-flow between the layers as a result of the contrast in capillary pressure and the influence of the gravity. Table 5 and Figure 6 shows the performance of the proposed method with respect to the different injection and production wells and capillary pressure parameters. It is clearly seen that the simulation spends more computing time when the capillary pressure is used, which attributes to the increase in nonlinearity of the problem that affects the size of time step. We remark that the additional step introduced in Remark 2 is not triggered when the capillary pressure is ignored.

Table 5: A comparison of different capillary pressure parameters for Case-4. The mesh is 220×60, the time step size is fixed to $\triangle t = 0.01$. The simulation is stopped at $t = 6$.

Model	Model-1		Model-2	
Capillary pressure	$B_c = 0$	$B_c = 20$	$B_c = 0$	$B_c = 20$
Average nonlinear iteration	1.12	5.84	1.06	5.78
Average linear iteration	31.85	23.97	68.51	66.07
Execution time (second)	66.84	296.08	90.49	371.93

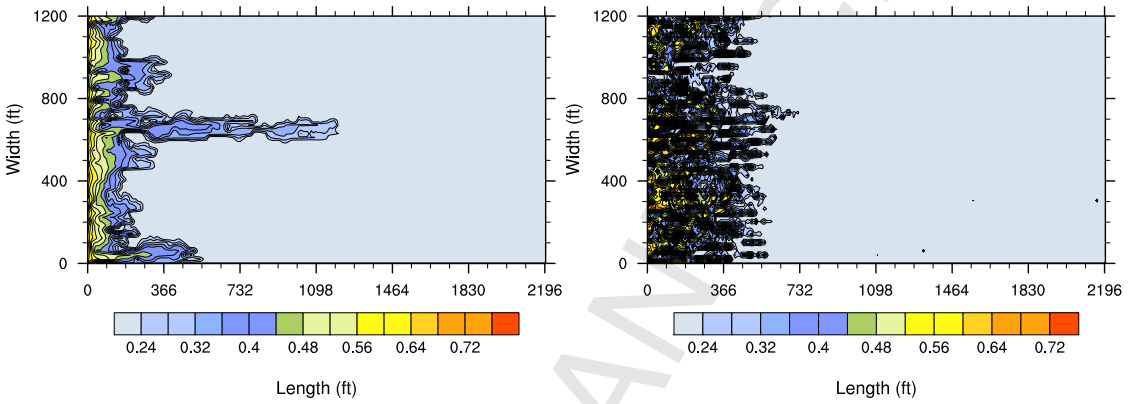

(a) Model-1 with $B_c = 0$

(b) Model-1 with $B_c = 20$

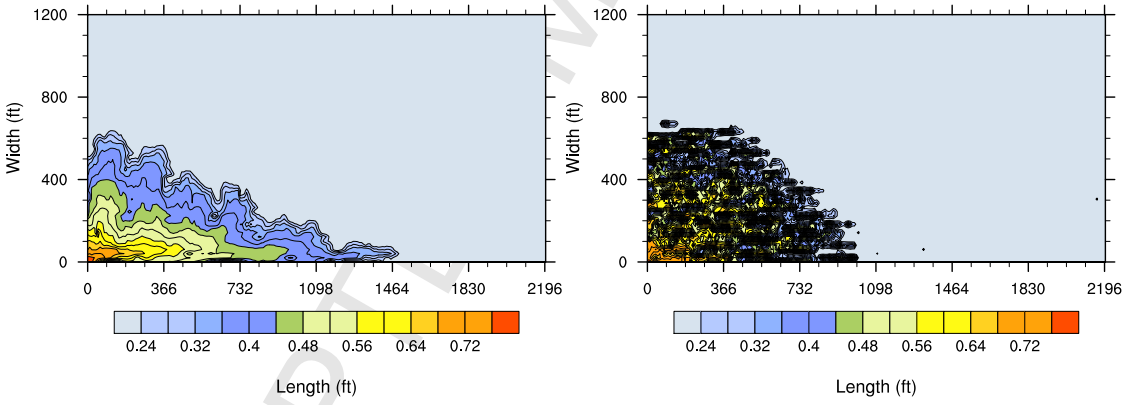

(c) Model-2 with $B_c = 0$

(d) Model-2 with $B_c = 20$

Figure 6: Wetting-phase saturation profiles with different B_c for Case-4. The mesh is 220×60, the time step size is fixed to $\triangle t = 0.01$. The simulation is stopped at $t = 6$.

4.3. Effect of adaptive time stepping

In the fifth test case (Case-5), we consider a 3D domain with a 300 m × 150 m × 150 m dimension and a random distribution of permeability with the range $[0.0013, 161.6361]$, which are generated by the open source code MRST (MATLAB Reservoir Simulation Toolbox) [28]. The densities are $\rho_w^{\text{ref}} = 1000\text{kg/m}^3$ and $\rho_n^{\text{ref}} = 600\text{kg/m}^3$. In the test, the porosity of this medium is 0.2; the viscosities of water and oil are 1 cP and 0.2 cP, respectively; the relative permeability is $\beta = 2$; and the injection rate is 0.1 PV/year. The capillary pressure function B_c is equal to 25 md. The injection and production wells are the same as in Case-3.

In the reservoir simulation, the equations (1) can enable different time scales that change in orders of magnitudes as the evolution of the dynamical system. Hence, it is often practical to use an adaptive time step size during the entire simulation, especially when the long-time simulation of the two-phase flow is of interest. In this test, we compare the performance of the fully implicit method when the adaptive stepping mechanism is applied or not. The mesh is $100 \times 50 \times 50$ and the simulation is stopped at $t = 1.5$. In the adaptive method, we set the initial time step size to be $\triangle t = 0.01$ year and then adaptively control it by using the mechanism (A.1); while, in the standard method, the time step size is fixed to $\triangle t = 0.01$ year. From Table 6, it is clear that the time step size of the adaptive method is far larger than that of the standard method, and the total computing time of the adaptive method is also much smaller than that of the standard method. In addition to that, even with large time step sizes, the fully implicit method with adaptive time stepping has a similar accuracy as the fully implicit method with a fixed, small time step size, as shown in Figure 7.

Table 6: A comparison of the fixed and adaptive time stepping for Case-5.

Method	Adaptive	Fixed
Number of time steps	267	1500
Average time step size (years)	5.62×10^{-3}	10^{-3}
Average nonlinear iteration	3.03	2.04
Average linear iteration	76.46	49.26
Execution time (second)	851.13	1621.92

4.4. Parallel performance

The purpose of this last example (Case-6) is to show the parallel performance of the proposed fully implicit method. We consider a 3D domain with dimension (300 m × 150 m × 150 m). The permeabilities are defined by

$$k = \begin{cases} 1 \text{ md} & 50 \le y \le 100 \text{ and } 50 \le z \le 100, \\ 100 \text{ md} & \text{otherwise.} \end{cases}$$

The injection and production wells are located at the right and left sides, respectively. The injection rate is 0.01 PV/year. The rock and fluid are the same as Case-3.

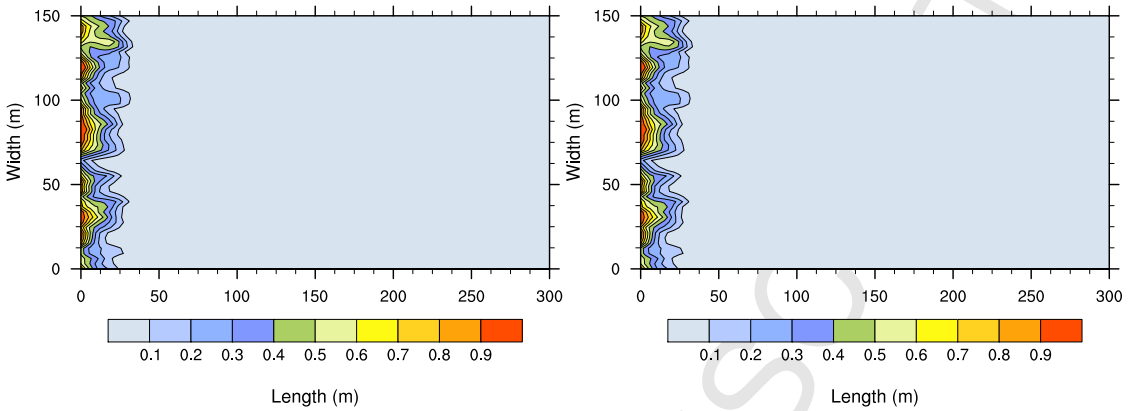

(a) Fixed and layer=1

(b) Adaptive and layer=1

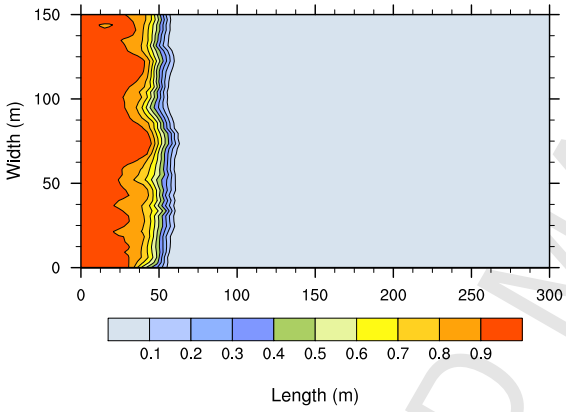

(c) Fixed and layer=30

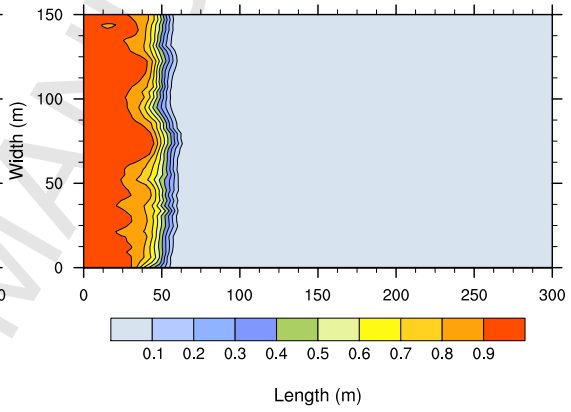

(d) Adaptive and layer=30

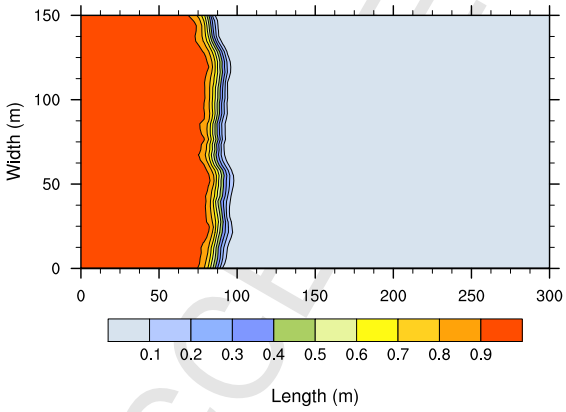

(e) Fixed and layer=50

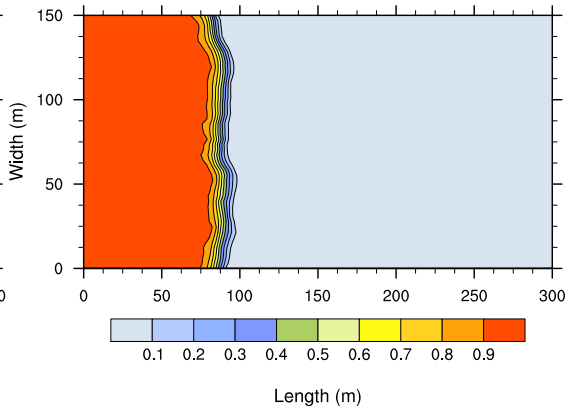

(f) Adaptive and layer=50

Figure 7: Wetting-phase saturation profiles with the fixed and adaptive time stepping for Case-5. We use the logarithmic scale for the permeability, i.e., $\log(k)$ where k has a unit of md. In the figure, "layer" denotes the layer of the mesh size in the z-direction.

We first investigate the performance of the fully implicit solver when different types of the additive Schwarz preconditioners are employed and when different overlaps are taken. Here, we test the classical-AS (18), the left-RAS (19), and the right-RAS (20) preconditioners. For each numerical case, the overlapping size δ in additive Schwarz methods is gradually increased from 0 to 3. As shown in Table 7, the performance results are listed by means of number of time steps, the numbers of iterations as well as the total compute time. In the test, the mesh is $100 \times 50 \times 50$, the initial time step size is used to $\triangle t = 10^{-3}$. The simulation is stopped at $t = 0.2$. Observations can be made from the table that: (a) the number of time steps and Newton iterations are always insensitive to the overlapping size δ in the tests, except the classical-AS; (b) for a given type of the AS preconditioner, the number of linear iterations decreases as δ becomes larger and the fastest compute time is obtained when $\delta = 1$; and (c) for a fixed δ, among the three additive Schwarz preconditioners, the right-RAS preconditioner gets a best performance while the classical preconditioner performs the worst, in terms of both the number of linear iterations and the total compute time. We remark that when the overlap is zero, all the Schwarz preconditioners degenerates to the block-Jacobi preconditioner. As a result, the performance of the three AS preconditioners is the same when $\delta = 0$.

Table 7: Performance with respect to the overlapping factor δ for Case-6. The number of processors is $N_p = 144$.

AS-type	Overlapping size δ	0	1	2	3
Classical-AS	Number of time steps	28	28	28	28
	Average nonlinear iteration	3.07	3.14	3.11	3.07
	Average linear iteration	87.2	69.9	61.5	52.8
	Execution time (second)	67.9	65.6	104.3	305.5
Left-RAS	Number of time steps	28	28	28	28
	Average nonlinear iteration	3.07	3.07	3.07	3.07
	Average linear iteration	87.2	48.9	36.6	30.6
	Execution time (second)	67.9	56.9	86.5	140.9
Right-RAS	Number of time steps	28	28	28	28
	Average nonlinear iteration	3.07	3.07	3.07	3.07
	Average linear iteration	87.2	48.3	35.2	28.5
	Execution time (second)	67.9	56.0	84.6	138.2

In the following, we numerically investigate the scalability of the proposed fully implicit solver for Case-6 in terms of the nonlinear and linear iterations, and the computing time. The definition of the scalability is $Speedup = T_1/T_2$, where T_1 and T_2 are the execution times obtained by running the parallel code with $N_{p,1}$ and $N_{p,2}$ processors ($N_{p,1} \leq N_{p,2}$), respectively. We also report the parallel efficiency by $E_f = (N_{p,1} \times T_1)/(N_{p,2} \times T_2)$. In the test, the simulation is stopped after ten implicit time steps with a $256 \times 128 \times 128$ mesh. The initial time step size is used to $\triangle t = 10^{-5}$. The simulation is stopped after 10th implicit time steps. Table 8 shows the number of nonlinear and linear iterations as well as the computing time with respect to the number of processors. We can see that the number

of nonlinear iterations per time step is independent of the number of processors, and the number of linear iterations grows slowly with the increase of the number of processors.

Table 8: Scalability with different numbers of processors N_p for Case-6.

Number of processors	256	512	1024	2048
Average nonlinear iteration	3.8	3.8	3.8	3.8
Average linear iteration	89.6	106.2	118.4	154.5
Execution time (second)	1165.6	518.7	261.1	158.3
Speedup	1.00	2.25	4.46	7.36
Efficiency	100.0%	112.3%	111.6%	92.0%

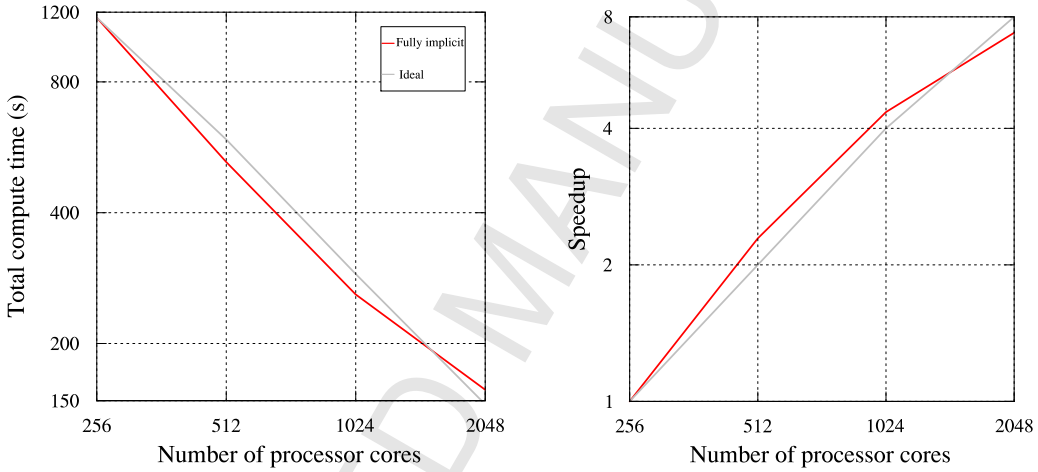

Figure 8: Scalability results with different number of processors N_p for Case-6.

5. Concluding remarks

In this paper, a fully implicit scheme and a highly parallel domain decomposition based preconditioning technique are proposed for solving the two-phase flow in a porous medium with capillarity, gravity and compressibility. The proposed fully implicit scheme can get rid of the restriction of the time step size, which is derived based on the mixed finite element method and implicit Backward Euler method. Moreover, an adaptive time stepping strategy is successfully incorporated into the proposed time integration scheme so that the time step size is controlled based on the state of solution. The nonlinear system arising from the discretization of the two-phase flow problem at each time step is solved by the Newton–Krylov framework. The accuracy and applicability of the proposed method are validated by several one, two and three dimensional test cases.

Acknowledgements

The authors would like to express their appreciations to the anonymous reviewers for the invaluable comments that have greatly improved the quality of the manuscript. The work was supported in part by the National Natural Science Foundation of China (11571100) and the state key laboratory program of LASG (20170062). S. Sun was also supported by KAUST through the grant BAS/1/1351-01-01.

Appendix A.

In the Appendix, we introduce a fully implicit scheme for the two-phase slightly compressible flow. In this paper, we employ a mixed finite element method (MFEM) for the spatial discretization. We partition the domain Ω by a finite number of mesh cells. For the pressure unknown, the finite element space we use is Q_κ, which is the space of piecewise tensor-product polynomials of order κ. For the velocity unknown, we approximate $\hat{u}_\alpha := u_\alpha/(k_{r\alpha}\rho_\alpha)$ using the Raviart-Thomas space RT_κ. Here we solve $\hat{u}_\alpha$ as the direct unknown instead of the original mass flux rate $u_\alpha = k_{r\alpha}\rho_\alpha\hat{u}_\alpha$. We note that the Raviart-Thomas space RT_κ of order κ is the smallest polynomial space such that the divergence maps RT_κ onto Q_κ. The work can be extended to higher-order $\kappa \geq 1$, but we consider only the lowest-order approximation (i.e. $\kappa = 0$) in the numerical examples of this paper. We denote the finite-dimensional velocity space (which vanishes on Γ_N) by $\mathbf{V}_h \subset \mathrm{RT}_\kappa$; and denote the finite-dimensional pressure space by $W_h = \mathrm{Q}_\kappa$. The continuous-in-time algorithm reads: Find $S_w(\cdot,t) \in W_h$, $S_o(\cdot,t) \in W_h$, $p_w(\cdot,t) \in W_h$, $p_o(\cdot,t) \in W_h$, $\hat{u}_w(\cdot,t) \in V_h$, and $\hat{u}_o(\cdot,t) \in V_h$, such that

$$
\begin{aligned}
\left(\frac{\partial}{\partial t}(\phi\rho_\alpha S_\alpha), w\right) + \langle k^*_{r\alpha}\rho^*_\alpha\hat{u}_\alpha\cdot n, w\rangle_{\Gamma_D} - (k_{r\alpha}\rho_\alpha\hat{u}_\alpha, \nabla w) &= (q_\alpha, w)\,,\ \alpha = o, w,\ \forall w \in W_h,\\
\left(\mu_\alpha\mathbf{K}^{-1}\hat{u}_\alpha, v\right) - (p_\alpha, \nabla v) + \langle p_\alpha, v\cdot n\rangle_{\Gamma_D} + (\rho_\alpha g\nabla z, v) &= 0,\ \alpha = o, w,\ \forall v \in V_h,\\
(S_o + S_w, w) &= 0,\ \forall w \in W_h,\\
(p_o - p_w, w) &= (p_c(S_w), w)\,,\ \forall w \in W_h.
\end{aligned}
$$

Here, $k^*_{r\alpha}$ and ρ^*_α represent the upwind values of $k_{r\alpha}$ and ρ_α based on the direction of the velocity $\hat{u}_\alpha$. Note that we use the Raviart-Thomas space RT_κ to approximate $\hat{u}_\alpha$ instead of u, because $\hat{u}_\alpha$ is a smooth function while u can be a function with discontinuities or sharp gradients.

Using the trapezoidal quadrature rule, the velocity unknowns in the system above can be eliminated. Using the saturation summation constraint and the capillary pressure relation, we can also eliminate S_o and p_o. This results in only two primary unknowns (S_w and p_w) for the system. To get a fully discretized system, we adopt the implicit backward Euler scheme with adaptive time stepping for the temporal integration. More precisely, we adaptively control the time step size $\triangle t^{(m)}$ by using a switched evolution/relaxation strategy, to handle physically meaningful simulations and meanwhile reduce the computational cost. In the

approach, we start with a relatively small time step size $\triangle t^{(0)}$ and then update its value according to

$$\triangle t^{(m)} = \max\left\{1/\alpha, \min\{\alpha, \beta\}\right\} \triangle t^{(m-1)}, m = 1, 2, \cdots \tag{A.1}$$

where $\alpha > 1$ is used to avoid excessive change of the time step size between any two immediate time steps, and β is given by

$$\beta = \left(\|r^{(m-1)}\|_2 / \|r^{(m)}\|_2\right)^{\gamma},$$

where $0 < \gamma < 1$ is a parameter to control the adjustment of the time step size and $\|r^{(m)}\|_2$ is the Euclidean norm of the function arising from the discretization of (1).

References

[1] K. Aziz, A. Settari, Petroleum Reservoir Simulation, Applied Science Pub. London, 1979.

[2] S. Balay, J. Brown, K. Buschelman, V. Eijkhout, W. Gropp, D. Kaushik, M. Knepley, L. C. McInnes, B. F. Smith, H. Zhang, PETSc Users Manual, Argonne National Laboratory, 2016.

[3] S. J. Benson, T. S. Munson, Flexible complementarity solvers for large-scale applications, Optim. Methods Softw. 21 (2006) 155–168.

[4] P. Brune, M. Knepley, B. Smith, X. Tu, Composing scalable nonlinear algebraic solvers, SIAM Review 57 (2015) 535–565.

[5] X.-C. Cai, M. Dryja, M. Sarkis, Restricted additive Schwarz preconditioners with harmonic overlap for symmetric positive definite linear systems, SIAM J. Numer. Anal. 41 (2003) 1209–1231.

[6] X.-C. Cai, W.D. Gropp, D.E. Keyes, R.G. Melvin, D.P. Young, Parallel Newton–Krylov–Schwarz algorithms for the transonic full potential equation, SIAM J. Sci. Comput. 192 (1998) 46–65.

[7] X.-C. Cai, M. Sarkis, A restricted additive Schwarz preconditioner for general sparse linear systems, SIAM J. Sci. Comput. 21 (1999) 792–797.

[8] Z. Chen, G. Huan, B. Li, An improved IMPES method for two-phase flow in porous media, Transport Porous Med. 54 (2004) 361–376.

[9] Z. Chen, G. Huan, Y. Ma, Computational Methods for Multiphase Flows in Porous Media, SIAM, Philadelphia, PA, 2006.

[10] D.A. Collins, L.X. Nghiem, Y.K. Li, J.E. Grabenstetter, An efficient approach to adaptive implicit compositional simulation with an equation of state, SPE Reservoir Engineering, 7 (1992) 259–264.

[11] K.H. Coats, IMPES stability: the CFL limit, presented at the SPE Reservoir Simulation Symposium, Houston, TX. Mar. 2001, SPE 85956.

[12] K.H. Coats, IMPES stability: selection of stable time steps, presented at the SPE Reservoir Simulation Symposium, Houston, TX. Feb. 2001, SPE 84924.

[13] M. Christie, M. Blunt, Tenth SPE comparative solution project: A comparison of upscaling techniques. In SPE Reservoir Simulation Symposium. Society of Petroleum Engineers. (2001) 308–317.

[14] C.N. Dawson, H. Klíe, M.F. Wheeler, C.S. Woodward, A parallel, implicit, cell-centered method for two-phase flow with a preconditioned Newton–Krylov solver, Computat. Geosci. 1 (1997) 215–249.

[15] C. Dawson, S. Sun, M.F. Wheeler, Compatible algorithms for coupled flow and transport, Comput. Meth. in Appl. Mech. and Engng. 193(2004) 2565–2580.

[16] V. Dolean, S. Lanteri, F. Nataf, Convergence analysis of additive Schwarz for the Euler equations, Appl. Numer. Math. 49 (2004) 153–186.

[17] M. Dryja, O.B. Widlund, Domain decomposition algorithms with small overlap, SIAM J. Sci. Comput. 15 (1994) 604–620.

[18] S.C. Eisenstat, H.F. Walker, Globally convergent inexact Newton method, SIAM J. Optim. 4 (1994) 393–422.

[19] V.J. Ervin, E.W. Jenkins, S. Sun, Coupled generalized non-linear Stokes flow with flow through a porous medium, SIAM J. Numer. Anal. 47(2009) 929–952.

[20] R.G. Fagin, C.H. Jr. Stewart, A new approach to the two-dimensional multiphase reservoir simulator, SPE J, 1966, SPE 1188.
[21] W.D. Gropp, D.K. Kaushik, D.E. Keyes, B.F. Smith, High-performance parallel implicit CFD, Parallel Comput. 27 (2001) 337–362.
[22] W.D. Gropp, D.E. Keyes, L. McInnes, M. Tidriri, Globalized Newton–Krylov–Schwarz algorithms and software for parallel implicit CFD, Int. J. High Perform. Comput. Appl. 14 (2000) 102–136.
[23] M. Hintermüller, K. Ito, K. Kunisch, The primal-dual active set strategy as a semismooth Newton method, SIAM J. Optim. 13 (2003) 865–888.
[24] H. Hoteit, A. Firoozabadi, Numerical modeling of two-phase flow in heterogeneous permeable media with different capillarity pressures, Adv. Water Resour. 31 (2008) 56–73.
[25] D.A. Knoll, D.E. Keyes, Jacobian-free Newton–Krylov methods: A survey of approaches and applications, J. Comput. Phys. 193 (2004) 357–397.
[26] J. Kou, S. Sun, A new treatment of capillarity to improve the stability of IMPES two-phase flow formulation, Comput. Fluids 39 (2010) 1293–1931.
[27] S. Lacroix, Y.V. Vassilevski, J.A. Wheeler, M.F. Wheeler, Iterative solution methods for modeling multiphase flow in porous media fully implicitly, SIAM J. Sci. Comput. 25 (2003) 905–926.
[28] K. Lie, S. Krogstad, I. Ligaarden, J. Natvig, H. Nilsen, B. Skaflestad, Open-source MATLAB implementation of consistent discretisations on complex grids, Comput. Geosci. 16 (2012) 297–322.
[29] B. Lu, Iteratively Coupled Reservoir Simulation for Multiphase Flow in Porous Media, PhD dissertation, The University of Texas at Austin, 2008.
[30] B. Lu, M. F. Wheeler, Iterative coupling reservoir simulation on high performance computers, Pet. Sci. 6 (2009) 43–50.
[31] J.E.P. Monteagudo, A. Firoozabadi, Comparison of fully implicit and IMPES formulations for simulation of water injection in fractured and unfractured media, Int. J. Numer. Meth. Engng. 69 (2007) 698–728.
[32] J. Moortgat, S. Sun, A. Firoozabadi, Compositional modeling of three-phase flow with gravity using higher-order finite element methods, Water Resources Res. 47(2011) W05511.
[33] Y. Saad, Iterative Methods for Sparse Linear Systems. SIAM, Second ed., 2003.
[34] J.O. Skogestad, E. Keilegavlen, J.M. Nordbotten, Domain decomposition strategies for nonlinear flow problems in porous media, J. Comput. Phys. 234 (2013) 439–451.
[35] B. Smith, P. Bjørstad, W. Gropp, Domain Decomposition: Parallel Multilevel Methods for Elliptic Partial Differential Equations, Cambridge University Press, 1996.
[36] S. Sun, M.F. Wheeler, Symmetric and nonsymmetric discontinuous Galerkin methods for reactive transport in porous media, SIAM J. Numer. Anal. 43(2005) 195–219.
[37] S. Sun, M.F. Wheeler, L2(H1) norm a posteriori error estimation for discontinuous Galerkin approximations of reactive transport problems, J. Sci. Comput. 22(2005), 501–530.
[38] S. Sun, M.F. Wheeler, Discontinuous Galerkin methods for coupled flow and reactive transport problems, AAppl. Numer. Math. 52(2005): 273–298.
[39] T.B. Tan, N. Kaiogerakis, A fully implicit, three-dimensional, three-phase simulator with automatic history-matching capability, presented at the 11th SPE Symposium on Reservoir Simulation, Anaheim, CA. Feb. 1991, SPE 21205.
[40] A. Toselli, O. Widlund, Domain Decomposition Methods-Algorithms and Theory, Springer, Berlin, 2005.
[41] K. Wang, H. Liu, Z. Chen, A scalable parallel black oil simulator on distributed memory parallel computers, J. Comput. Phys. 301 (2015) 19–34.
[42] Y. Wu, K. Pruess, and Z. Chen. Buckley-Leverett Flow in Composite Porous Media. SPE Advanced Technology Series, 1 (1993) 1990–1991.
[43] C. Yang, X.-C. Cai, A scalable fully implicit compressible Euler solver for mesoscale nonhydrostatic simulation of atmospheric flows, SIAM J. Sci. Comput. 35 (2014) S23–S47.
[44] H. Yang, S. Sun, C. Yang, Nonlinearly preconditioned semismooth Newton methods for variational inequality solution of two-phase flow in porous media, J. Comput. Phys. 332 (2017), 1-20.

[45] H. Yang, C. Yang, X.-C. Cai, Parallel domain decomposition methods with mixed order discretization for fully implicit solution of tracer transport problems on the cubed-sphere, J. Sci. Comput. 61 (2014) 258–280.
[46] H. Yang, C. Yang, X.-C. Cai, Mixed order discretization based two-level Schwarz precondtioners for a tracer transport problem on the cubed-sphere, Comp. Fluids 110 (2015) 88–95.
[47] H. Yang, C. Yang, S. Sun, Active-set reduced-space methods with nonlinear elimination for two-phase flow problems in porous media, SIAM J. Sci. Comput. 38 (2016) B593–B618.
[48] L.C. Young, R.E. Stephenson, A generalized compositional approach for reservoir simulation, SPE J. 23 (1983) 727–742.
[49] A. Zidane, A. Firoozabadi, An implicit numerical model for multicomponent compressible two-phase flow in porous media, Adv. Water Resour. 85 (2015) 64–78.